Section 7

Global and regional climate models, sensitivity and impact experiments, response to external forcing

Benchmarking Deep Soil Simulator against permafrost thermal characteristics measurements

M.M. Arzhanov, S.N. Denisov, V.S. Kazantsev
A.M. Obukhov Institute of Atmospheric Physics RAS, 3, Pyzhevsky, 119017 Moscow, Russia
arzhanov@ifaran.ru

Results of simulation and observations of the permafrost thermal state in the north of the West Siberia is compared. To simulate of soil state, off-line numerical experiments are performed with the Deep Soil Simulator (DSS) [1, 2]. The DSS is forced by the air temperature and snow depth (shown the red lines in Fig. 1) for 01.2012-12.2013.

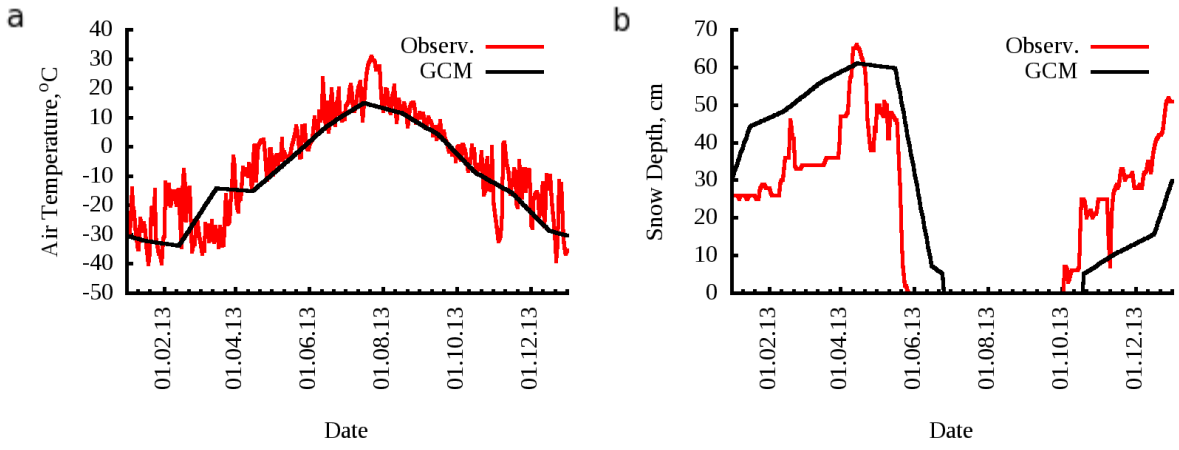

Fig. 1. Simulated using MIROC5 GCM (black lines) and measured at the Tazovskiy weather station (red lines) air temperature (a) and snow depth (b), respectively.

The daily means these meteorological parameters are calculated using the archive of the Tazovskiy weather station WMO ID 23256 (67°28'N, 78°43'E) (http://rp5.ru). The active layer thickness (ALT) and soil temperature is measured at experimental site of the tundra zone (67°22'N, 78°37'E) for 07.2013-10.2013 [3]. Simulated and measured soil temperatures at 1.5 m and 3 m are shown in Fig. 2a. The active layer thickness are shown in Fig. 2b. Simulated values are in the good agreement with the measured.

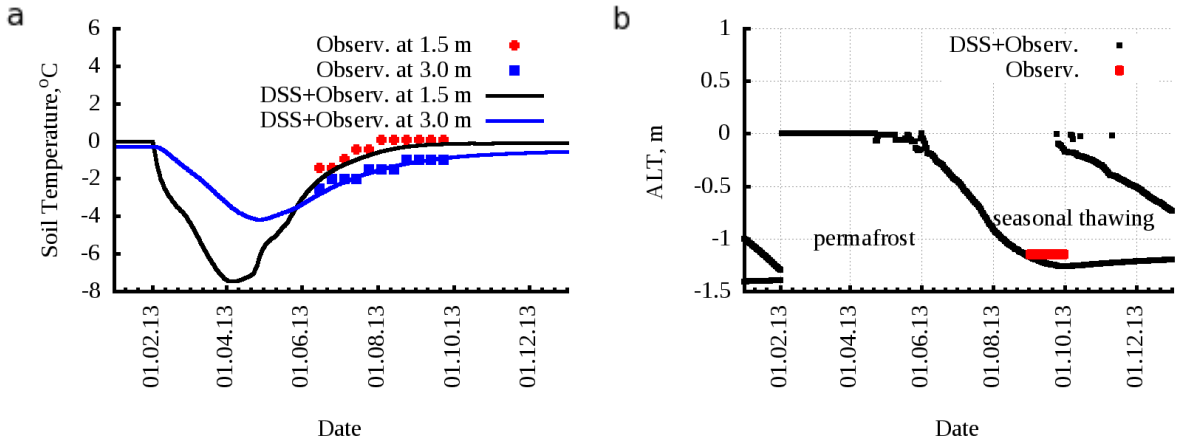

Fig. 2. Simulated and measured soil temperatures at 1.5 m and 3 m (a) and active layer thickness (b).

To assess the soil regime dynamics during the 21st century the DSS is forced by the MIROC5 GCM air temperature and snow depth under RCP 8.5 anthropogenic scenario. Comparison of simulated and observed values of these parameters is shown in Fig. 1. Results of numerical experiments with DSS forced by the MIROC5 GCM are shown in Fig. 3. Simulated soil thermal regime is changed since 2060s (Fig. 3a). Soil thaw depth increased from the 2010s to the 2060s (Fig. 3b). For this experimental site talik formation occurred about 2063-2064.

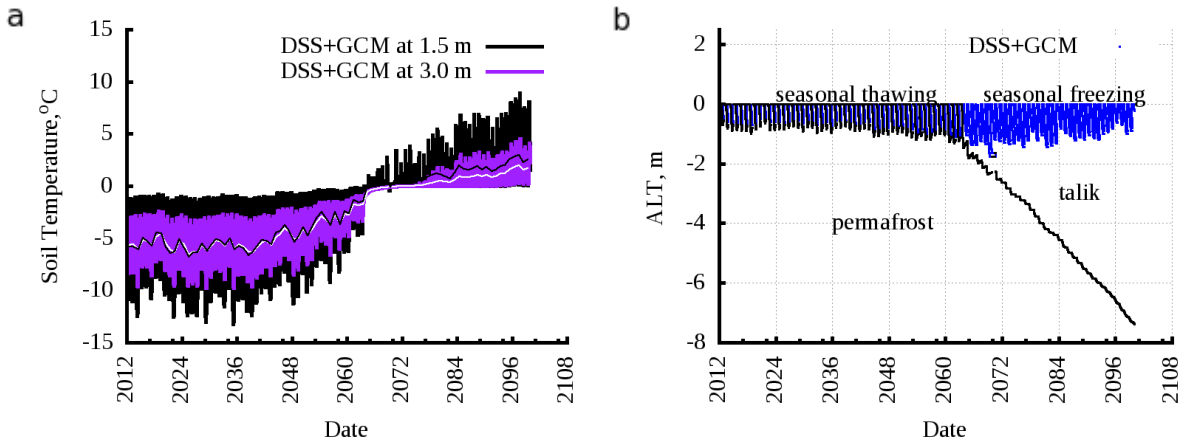

Fig. 3. Simulated yearly means and amplitudes of the soil temperatures at 1.5 m (black line) and 3 m (purple line) (a) and active layer thickness (b) for 2012-2100.

Acknowledgements

The Russian Fondation for Basic Research (12-05-01092, 14-05-00193, 14-05-93089, 14-05-00518, 12-05-91323-SIG), The program of the Earth Sciences Department of the Russian Academy of Sciences, Programs of the Russian Ministry for Science and Education (contracts 8833).

References

1. Arzhanov M.M., Eliseev A.V., Demchenko P.F., Mokhov I.I., and Khon V.Ch. Simulation of Thermal and Hydrological Regimes of Siberian River Watersheds under Permafrost Conditions from Reanalysis Data // Izvestiya, Atmospheric and Oceanic Physics, 2008, Vol. 44, No. 1, pp. 83–89.

2. Arzhanov M.M., Eliseev A.V., Mokhov I.I. A global climate model based, Bayesian climate projection for northern extra-tropical land areas // Glob. Planet. Change. 2012. V.86-87. P.57-65.

3. Kazantsev V.S., Zarov E.A., Loyko S.V., Arzhanov M.M., Golubyatnikov L.L., Denisov S.N., Zavalishin N.N. Instrumental measurements of methane fluxes and stocks of soil organic in tundra ecosystems // XVII Russian Conference "Composition of the atmosphere. Atmospheric electricity. Climate Processes". N. Novgorod. 2013. p. 36.

RELATIONSHIP BETWEEN EL-NINO AND ASIAN SUMMER MONSOONS DURING LAST 9.5 KA FROM MODEL SIMULATIONS

V.C. Khon, I.S. Larkina, I.I. Mokhov and A.V. Timazhev

A.M. Obukhov Institute of Atmospheric Physics RAS, Moscow, Russia
khon@ifaran.ru

The aim of this study is to analyze the relationship between El Nino - Southern Oscillation (ENSO) and the Asian summer monsoon under changing orbital configuration over the last 9,500 years. The transient climate simulations with the Kiel Climate Model (KCM, Park et al., 2009) are used for analysis (see e.g. Jin et al., 2014). Two indices characterizing different regional subsystems of the ASM are analyzed. The Indian summer monsoon (ISM) was defined as the all-India rainfall during the summer (June-July-August). The East Asian summer monsoon (EASM) was defined according to Han and Wang (2007). The strength of ENSO phenomena is characterized by the sea surface temperature (SST) for the Nino3.4 region (e.g. Jin et al., 2014).

Figure 1 shows local coherence between the ISM and EASM indices from model simulations over the last 9,500 years. According to Fig. 1 south and east parts of the Asian monsoon system display both significant relationship and remarkable difference from long-term model simulations. A significant coherence is noted for variations with periods about 10^2 years with a less coherent variations near mid-Holocene (about 6000 years ago).

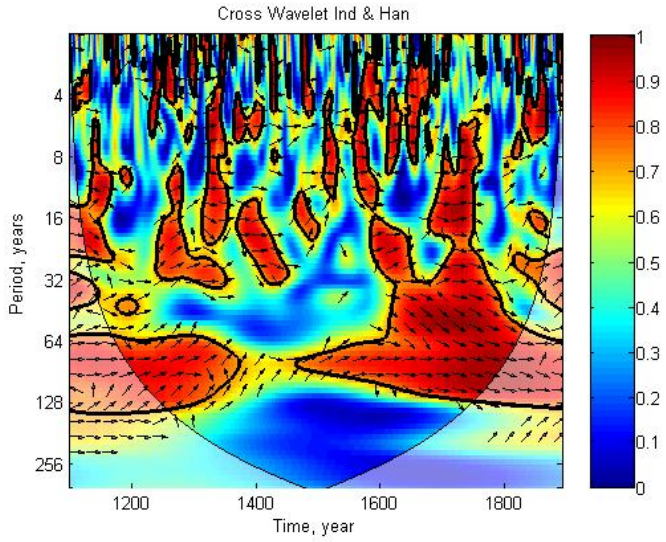

Figure 1. Wavelet coherence between ISM and EASM indices from model simulations for the last 9.5 ka. Direction of time axis begins at 9.5 ka BP towards the present.

Figures 2 and 3 show local coherence for Nino3.4 SST in December-January-February with EASM (Fig. 2) and ISM (Fig. 3) indices from model simulations over the last 9,500 years. The most significant coherence (with negative correlation) with the Nino3.4 SST is noted for variations with periods about 10^2 years of the EASM and ISM indices after mid-Holocene. No significant coherence was found for such variations between the ISM index and Nino3.4 SST before mid-Holocene.

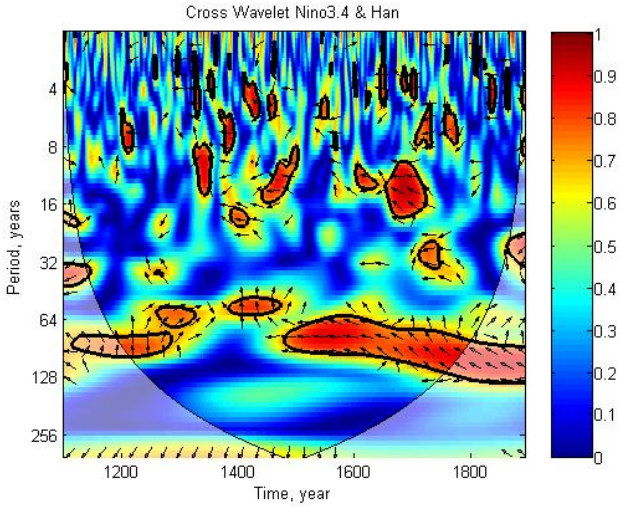

Figure 2. Wavelet coherence between Nino3.4 SST in December-January-February and EASM index from model simulations for the last 9.5 ka.

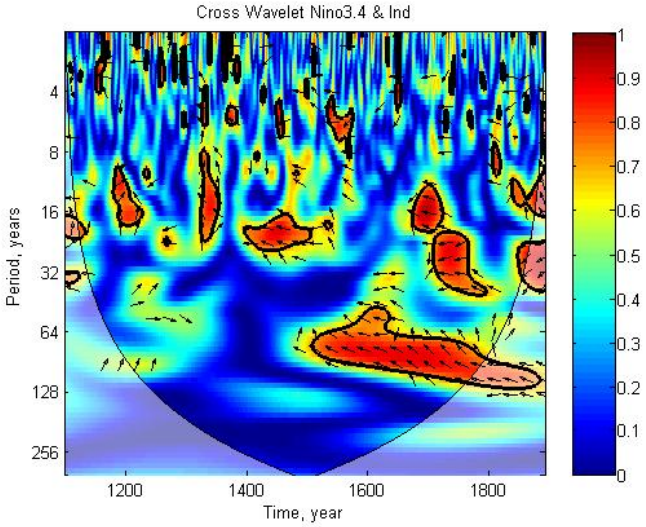

Figure 3. Wavelet coherence between Nino3.4 SST in December-January-February and ISM index from model simulations for the last 9.5 ka.

References

Han J. and H. Wang, 2007: Interdecadal variability of the East Asian summer monsoon in an AGCM. *Adv. Atmos. Sci.*, **24**, 808–818.

Jin L., B. Schneider, W. Park, M. Latif, V. Khon and X. Zhang, 2014: The spatial-temporal patterns of Asian summer monsoon precipitation in response to Holocene insolation change: a model-data synthesis. *Quatern. Sci. Rev.*, **85**, 47–62.

ParkW., N. Keenlyside, M. Latif, A. Stroeh, R. Redler, E. Roeckner and G. Madec, 2009: Tropical Pacific climate and its response to global warming in the Kiel Climate Model. *J. Clim.*, **22**, 71-92.

ATMOSPHERIC BLOCKINGS IN NORTHERN HEMISPHERE FROM MODEL SIMULATIONS WITH RCP SCENARIOS

I.I. Mokhov and A.V. Timazhev

A.M. Obukhov Institute of Atmospheric Physics RAS, Moscow, Russia
mokhov@ifaran.ru

Possible changes of atmospheric blocking characteristics in different regions of the Northern Hemisphere are evaluated from the CMIP5 simulations with the different RCP scenarios for the 21st century. Blocking characteristics were detected similar to (Wiedenmann et al., 2002; Mokhov et al., 2013).

Table 1(a,b) presents characteristics of summer (a) and winter (b) blockings in the Northern Hemisphere at the end of the 21st century (normalized to corresponding values for the 20th century - XX) from the IPSL-CM5B simulations with anthropogenic scenarios RCP 4.5 and RCP 8.5 for the 21st century: total blockings duration (blocking days number), mean blockings duration and mean blockings number for different longitudinal sectors and for hemisphere as a whole.

Table 1(a,b). Characteristics of summer (a) and winter (b) blockings in different longitudinal sectors and for the Northern Hemisphere as a whole at the end of the 21st century (normalized to corresponding values for the 20th century - XX) from the IPSL-CM5B simulations with anthropogenic scenarios RCP 4.5 and RCP 8.5 for the 21st century.

(a)

Blocking days number	180W-60W	60W-60E	60E-180E	NH
RCP 4.5 / XX	0.92	1.07	1.07	1.05
RCP 8.5 / XX	0.92	1.08	1.04	1.04
Mean duration	**180W-60W**	**60W-60E**	**60E-180E**	**NH**
RCP 4.5 / XX	0.79	0.93	0.86	0.88
RCP 8.5 / XX	0.97	0.99	1.11	1.03
Mean number	**180W-60W**	**60W-60E**	**60E-180E**	**NH**
RCP 4.5 / XX	1.14	1.14	1.24	1.19
RCP 8.5 / XX	0.93	1.08	0.93	1.01

(b)

Blocking days number	180E-60W	60W-60E	60E-180E	NH
RCP4.5/XX	1.19	1.04	0.84	1.03
RCP8.5/XX	0.95	1.07	0.90	1.01
Mean duration	**180E-60W**	**60W-60E**	**60E-180E**	**NH**
RCP4.5/XX	1.04	0.95	0.56	0.87
RCP8.5/XX	0.91	0.90	0.77	0.89
Mean number	**180E-60W**	**60W-60E**	**60E-180E**	**NH**
RCP4.5/XX	1.14	1.09	1.50	1.18
RCP8.5/XX	1.05	1.19	1.17	1.14

According to Table 1 it should be expected in the 21st century an overall increase in the frequency (the number of blocking days) and mean number of

summer and winter blockings in the Northern Hemisphere for both RCP scenarios.

Figure 1(a,b) shows the number of years (ordinate) with different blocking days (abscissa) for summer (a) and winter (b) in Euro-Atlantic region (60W-60E) from the IPSL-CM5B simulations for three 30-years periods: 1976-2005 (XX) and at the end of the 21st century (XXI) for the RCP 4.5 and RCP 8.5 scenarios.

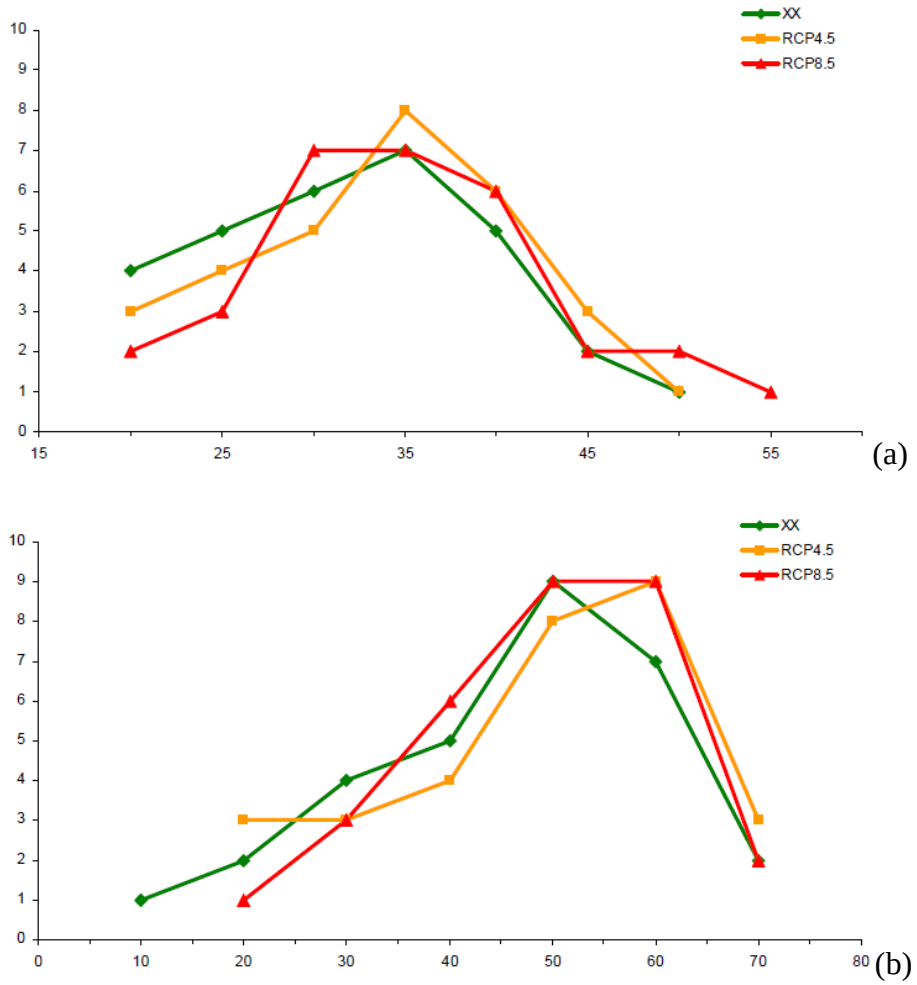

Figure 1(a,b). Number of years (ordinate) with different blocking days (abscissa) in Euro-Atlantic region for summer (a) and winter (b) from the IPSL-CM5B simulations for three 30-years periods: 1976-2005 (XX) and at the end of the 21st century (XXI) for the RCP 4.5 and RCP 8.5 scenarios.

According to Fig. 1 it should be expected in the 21st century more years with a greater number of blocking days in summer and winter in Euro-Atlantic region EA for both RCP scenarios.

References

Mokhov, I.I., M.G. Akperov, M.A. Prokofyeva, A.V. Timazhev, A.R. Lupo and H. Le Treut, 2013: Blockings in the Northern Hemisphere and Euro-Atlantic region: Estimates of changes from reanalysis data and model simulations. *Doklady Earth Sci.*, **449**(2), 430-433.

Wiedenmann J.M., A.R. Lupo, I.I. Mokhov and E.A. Tikhonova, 2002: The climatology of blocking anticyclones for the Northern and Southern Hemispheres: Block intensity as a diagnostic. *J. Climate*, **15**(23), 3459–3473.

Estimating time lags in a simple coupled climate-cabon cycle model

Muryshev K.E., Eliseev A.V.
A.M. Obukhov Institute of Atmospheric Physics RAS
kmuryshev@mail.ru, eliseev@ifaran.ru

The carbon dioxide exchange between the atmosphere, ocean, and land, in presence of periodic external forcing of different type is considered. The aim is to determine the delay between global temperature, concentration of atmospheric, and oceanic carbon stock.

The exchange of CO_2 between the atmosphere and the ocean is described by a Bacastow-type model but with a temperature-dependent chemical constants in the ocean. CO_2 fluxes from atmosphere to land ecosystems and ocean are determined by

$$G = \beta_L(q-q_0)+\gamma_L T ,$$
$$F = F_0 \chi (q - q_0 - \zeta Dq_0/D_0) ,$$

where T is deviation of global temperature from the initial value, q is concentration of CO_2 in the atmosphere, D is deviation of carbon stock at the ocean from its initial value $D_0 = 1.5*10^5$ PgC, $q_0 =$ 278 ppm, $\beta_L = (0.01 – 0.02)$ [GtC/ppm], $\gamma_L = 0.05$ [GtC/Kyear], and $F_0 = (2.5 – 4.5)$ [GtC/year] are coefficients, χ is the solubility of CO2 in the sea water, ζ is evasion factor.

The coupled climate-carbon system is governed by equations:

$$C_0(dq/dt) = E(t) – F – G ,$$
$$dD/dt = F ,$$
$$C\,(dT/dt) = p \ln(q/q_0) + R(t) – \lambda T,$$

where E(t) is external (e.g., anthropogenic) CO_2 emissions to the atmosphere, R(t) is temperature forcing, p= 5.34 [J/m^2 year], $C_0 = 2.123$ [GtC/ppm], C is heat capacity per unit area ($6*10^7$ J/m^2 K), λ is feedback factor (1.37 W/m^2 K).

The temperature and emission forcing for simplicity are in the form of a sinusoid with the period from one thousand to 10 thousand years. Forcing of this type produces oscillations of T, q, and D. We determined mutual delays between these variables by maxima of the lagged correlation between them.

When temperature forcing is applied, q lags T by about one hundred years. If the period of the external forcing is changed, the lag increases approximately in proportion to this period. At an emission forcing T is late concerning q for 1 year (a time step of the model).

References:

1. Boer G.J. and Arora V.K. (2013). Feedbacks in Emission-Driven and Concentration-Driven Global Carbon Budgets. *J. Climate*, **26**, 3326-3341.
2. Meier-Reimer E. and Hasselmann K. (1987). Transport and storage of CO2 in the ocean – an inorganic ocean-circulation carbon cycle model. *Climate Dynamics*, **2**, 63-90.

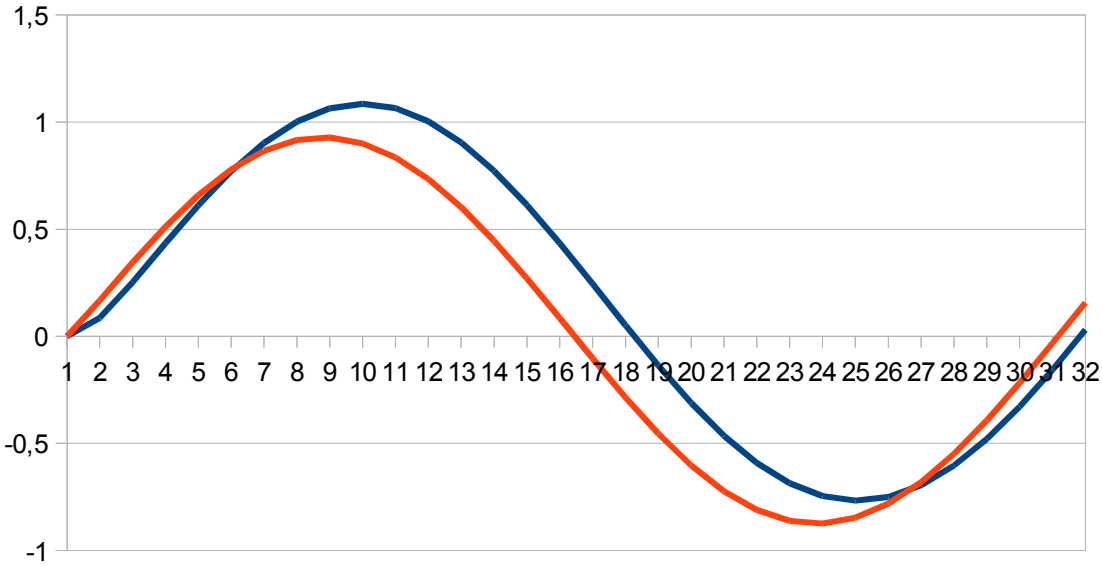

Figure 1. Time series of T [K] (red line) and q/q_0-1 (blue line) . Time is in centuries.

Stratospheric aerosols injections influence to global climate stabilization

V. P. Parkhomenko
Institution of Russian Academy of Sciences
Dorodnicyn Computing Centre of RAS
Moscow, Russia; parhom@ccas.ru

Global warming climate changes are observed in recent decades. These changes largely associated with anthropogenic increases in greenhouse gases in the atmosphere (CO_2 – most important among them) [1]. The problem and opportunity of the global climate stabilization [2] at a current level are investigated. The study is based on a three-dimensional hydrodynamic global climate coupled model, including ocean model with real depths and continents configuration, sea ice evolution model and energy and moisture balance atmosphere model [3, 4]. The climate prediction calculations up to the year 2100, using CO_2 growth scenario A2, proposed by IPCC are carried out on the first stage [5]. They give an increase in global mean annual surface air temperature at 2.2 degrees in the year 2100. Next, a series of calculations were carried out to assess the possibility of climate stabilization at the level of the year 2010 by controlling emissions into the stratosphere of aerosol, reflecting part of the incoming solar radiation. Aerosol concentration from the year 2010 up to 2100 is calculated as a controlling parameter to stabilize mean year surface air temperature. It is shown that by this way it is impossible to achieve the space and seasonal uniform approximation to the existing climate, although it is possible significantly reduce the greenhouse warming effect. Assumption of a uniform stratospheric aerosol space distribution can stabilize the mean atmosphere global temperature, but climate will be colder at 0.1-0.2 degrees in the low and mid-latitudes and at high latitudes it will be warmer at 0.2-1.2 degrees (Fig. 1, 2).

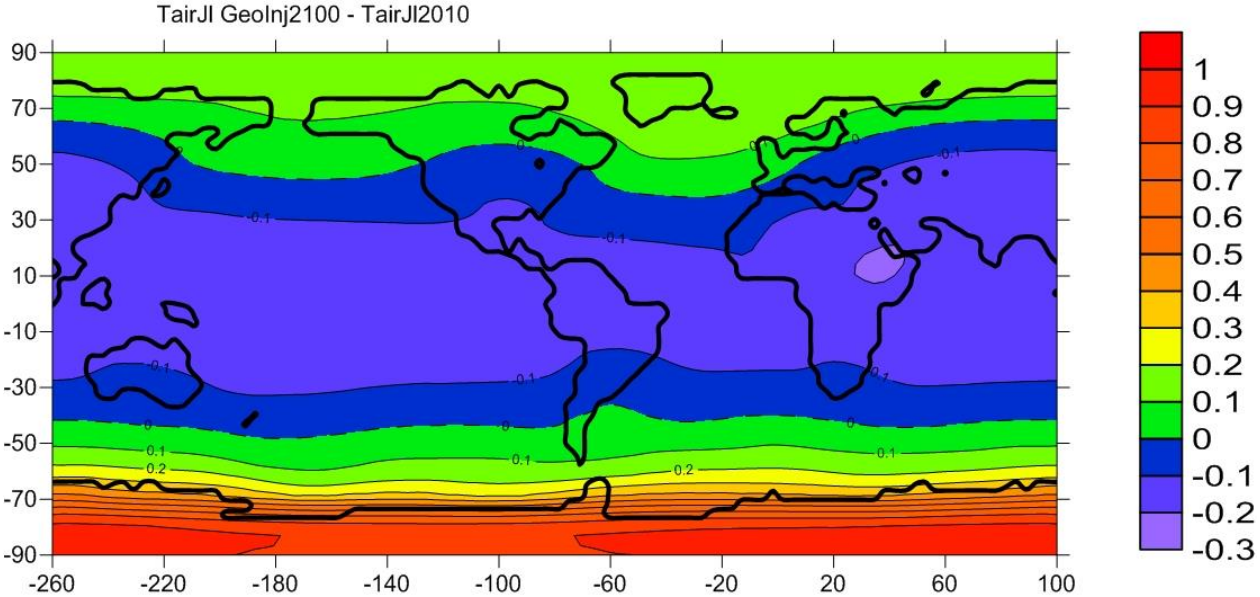

Fig.1. Difference between surface air temperature of stabilized climate (2100 year) and 2010 year climate. July

In addition, these differences have strong seasonal move – they increase in the winter season. The situation is slightly better when we allow latitude dependence of aerosol

concentrations. Compared to the previous case, the concentration is reduced in low and middle latitudes and is enlarged in high latitudes.

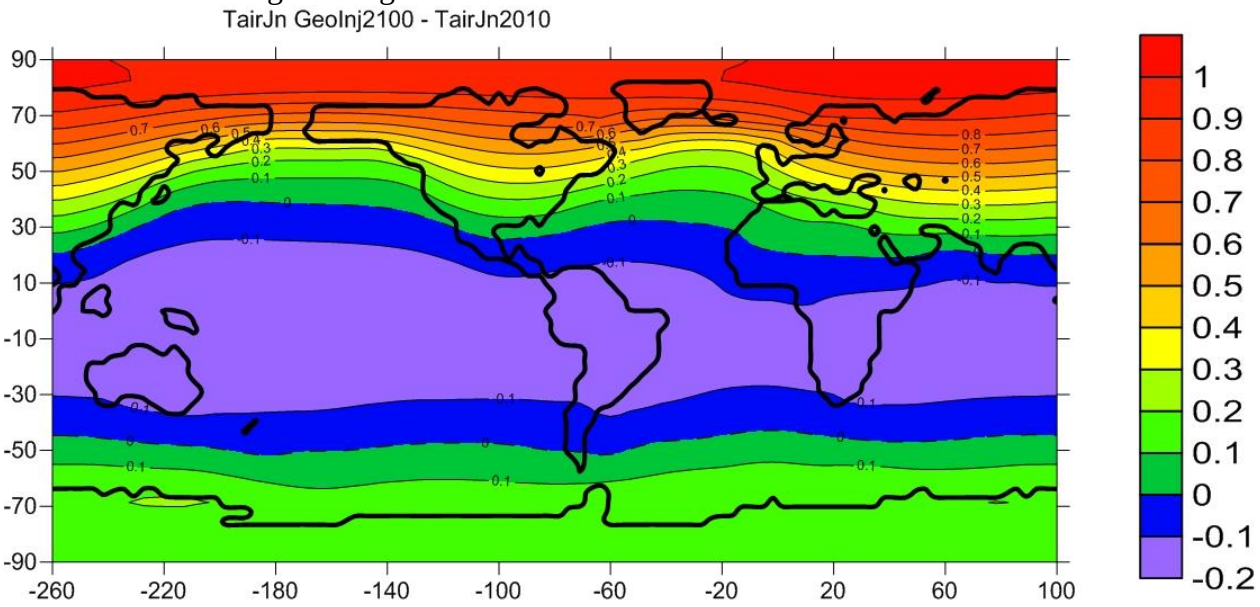

Fig.2. Difference between surface air temperature of stabilized climate (2100 year) and 2010 year climate. January

However, the increase in the aerosols concentration in the polar areas gives a weak effect, since there is little influence of solar radiation, while the greenhouse effect is stable. It is assumed in the following numerical experiments that aerosol emissions and concentration are zero from the year 2080. This leads to a rapid increase of the mean global atmospheric temperature, approaching the temperature without the aerosols to the year 2100.

The author was supported by the Russian Foundation for Basic Research (projects no. 14-01-00308, 14-07-00037) and Presidium RAS Basic Research Program (no. 14).

REFERENCES

1. “Climate Change 2007 – The physical Science Basis. Contribution of Working Group 1 to the Fourth Assessment Report of IPCC” . 2007, 989 p.

2. *Mercer A.M., Keith D.W., Sharp J.D.* // “Public understanding of solar radiation”. Management Environ. Res. Lett. 2011. V. 6. P. 1-9.

3. *Marsh R., Edwards N.R., Shepherd J.G.* “Development of a fast climate model (C-GOLDSTEIN) for Earth System Science.” // SOC, 2002, No.83. 54 p.

4. *V.P. Parkhomenko.* “Climate model with consideration World ocean deep circulation,” Vestnik MGTU im. Baumana. Issue Mathematical Modelling, p. 186-200 (2011) (in Russian).

5. *Nakicenovic N. et alI.* “IPCC Special Report on Emission Scenarios”, United Kingdom and New York, NY, USA, Cambridge University Press., 2000., 599 p.

Atmospheric Effects of the Earth's Monthly Motion

Nikolay S. Sidorenkov* and Taras S. Zhigailo**
* Hydrometeorological Research Center of the Russian Federation, Moscow
* Odessa State Environmental University, Ukraine
sidorenkov@mecom.ru

It is well known that the Earth and the Moon rotate around their center of mass (barycenter) with a sidereal period of 27.3 days. The orbit of the Earth's center of mass (geocenter) is geometrically similar to the Moon's orbit, but the orbit size is roughly 1/81 as large as that of the latter. The geocenter is, on average, 4671 km away from the barycenter. In the Earth's rotation around the barycenter, all its constituent particles trace the same nonconcentric orbits and undergo the same centrifugal accelerations as the orbit and acceleration of the geocenter. The Moon attracts different particles of the Earth with a different force. The difference between the attractive and centrifugal forces acting on a particle is called the tidal force [1]. The generation of the lunar tidal force is a major geophysical effect of the Earth's monthly motion. The rotation of the Earth–Moon system around the Sun (Fig. 1) leads to solar tides. The total lunisolar tides vary with a period of 355 days (13 sidereal or 12 synodic months). This period is known as the lunar or tidal year.

Importantly, the monthly orbit of the geocenter (like the orbit of the Moon) precesses with a period of 18.61 years and its perigee moves with a period of 8.85 years.

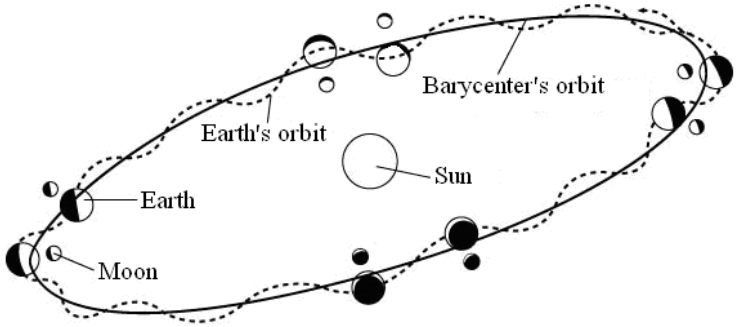

Fig. 1. Rotation of the Earth–Moon system around the Sun.

2. The lunisolar tides are believed to be so small that they cannot affect meteorological processes. In recent years, however, components of lunisolar tides have been detected in the spectra (a) of the atmospheric angular momentum, (b) of quasi-biennial oscillation indices of the equatorial stratospheric wind, and (c) of anomalies in many hydrometeorological characteristics [2]. It was found that synoptic processes vary simultaneously with tidal oscillations of the Earth's rotation rate and weather exhibits changes near their extrema, i.e., when the Earth is in certain positions on its monthly orbit [3].

An analysis of the causes of the 2010 anomalously hot summer in European Russia has revealed that the sunshine duration, cloud amount, and, eventually, the incoming solar radiation are modulated by lunar tides [4]. The intensity of the modulation depends on the season of the year. The length of the terrestrial (lunar) months is not a multiple of the solar year. The lunar (tidal) year, which is equal to 13 sidereal or 12 synodic months, lasts 355 days. Therefore, the incoming solar radiation varies not only with a solar year period of 365.24 days but also with a lunar or tidal year period of 355 days. Interference of these two oscillations with slightly different frequencies generates 35-year beats of incoming solar radiation, of the components of the Earth's radiation and heat budgets, and of the forcing of geophysical processes, such as the decade nonuniformity of Earth's rotation, decade climate changes, the El Niño–Southern

oscillation phenomenon, the intensity of the Indian monsoon, the state of the Antarctic ice sheet, etc. [4].

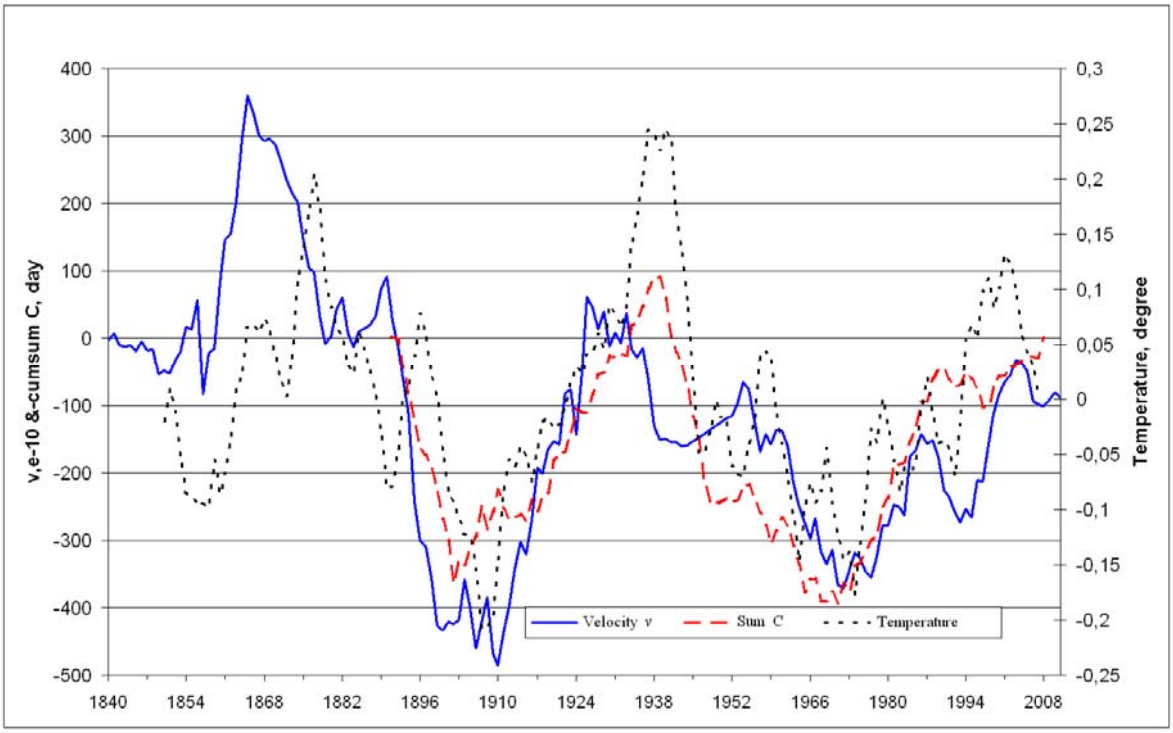

Fig. 2. Earth's rotation rate ν (solid), accumulated Vangengeim circulation pattern anomalies C taken with an opposite sign (dashed), and 5-year moving averages of anomalies in the global air temperature HadCRUT3: http://www.cru.uea.ac.uk/cru/data/temperature (dotted).

3. It was shown in [1, 2] that the Earth, the ocean, and the atmosphere exhibit consistent oscillations, influencing each other, i.e., joint oscillations initiated by tides occur in the Earth–ocean–atmosphere system. Visual manifestations of these oscillations include the wobble of the Earth's poles, El Niño and La Niña in the ocean, and the Southern Oscillation and the quasi-biennial oscillation in the atmosphere. The quasi-biennial oscillation (QBO) in the equatorial stratospheric wind direction has stability comparable with that of the annual period of meteorological element variations generated by the Earth's rotation around the Sun. The QBO period averaged over the last 60 years is equal to 28 months, or 2.3 years [1, 2].

The mechanism of QBO excitation is associated with the absorption of lunisolar tidal waves in the equatorial stratosphere. The QBO period is equal to a linear combination of the frequencies corresponding to the doubled periods of the tidal year (0.97 year), of the node motion (18.6 years), and of the perigee (8.85 years) of the Earth's monthly orbit:

$$\frac{1}{2}\left(\frac{1}{0.97}-\frac{1}{8.85}-\frac{1}{18.61}\right)=\frac{1}{2.3}$$

In other words, the quasi-biennial oscillation of the wind direction in the equatorial stratosphere is a combined oscillation caused by three periodic processes experienced by the atmosphere: (a) lunisolar tides, (b) the precession of the orbit of the Earth's monthly rotation around the barycenter of the Earth–Moon system, and (c) the motion of the perigee of this orbit.

References

1. N.S. Sidorenkov, *Physics of Instability in the Earth's Rotation* (Nauka, Moscow, 2002) [in Russian].
2. N.S. Sidorenkov, 2009: The interaction between Earth's rotation and geophysical processes. WILEY-VCH Verlag GmbH & Co. KGaA, Weinheim, 2009.
3. http://www.geoastro.ru
4. N. S. Sidorenkov and K. A. Sumerova, "Geodynamic causes of decade changes in climate," *Proc. Hydrometeorological Center of Russia*, 2012, Vol. 348, pp. 195–214.